This is an open access article published under a Creative Commons Attribution (CC-BY) License, which permits unrestricted use, distribution and reproduction in any medium, provided the author and source are cited.

ACS AUTHORCHOICE

JACS
JOURNAL OF THE AMERICAN CHEMICAL SOCIETY

pubs.acs.org/JACS

Article

Isolation of a Homoleptic Non-oxo Mo(V) Alkoxide Complex: Synthesis, Structure, and Electronic Properties of Penta-*tert*-Butoxymolybdenum

Julius Hillenbrand, Maurice van Gastel, Eckhard Bill, Frank Neese,* and Alois Fürstner*

Cite This: *J. Am. Chem. Soc.* 2020, 142, 16392−16402

Read Online

ACCESS | Metrics & More | Article Recommendations | Supporting Information

ABSTRACT: Treatment of $[MoCl_4(THF)_2]$ with MO*t*Bu (M = Na, Li) does not result in simple metathetic ligand exchange but entails disproportionation with formation of the well-known dinuclear complex $[(tBuO)_3Mo{\equiv}Mo(OtBu)_3]$ and a new paramagnetic compound, $[Mo(OtBu)_5]$. This particular five-coordinate species is the first monomeric, homoleptic, all-oxygen-ligated but non-oxo $4d^1$ Mo(V) complex known to date; as such, it proves that the dominance of the Mo=O group over (high-valent) molybdenum chemistry can be challenged. $[Mo(OtBu)_5]$ was characterized in detail by a combined experimental/computational approach using X-ray diffraction; UV/vis, MCD, IR, EPR, and NMR spectroscopy; and quantum chemistry. The recorded data confirm a Jahn−Teller distortion of the structure, as befitting a d^1 species, and show that the complex undergoes Berry pseudorotation. The alkoxide ligands render the disproportionation reaction, leading the formation of $[Mo(OtBu)_5]$ to be particularly facile, even though the parent complex $[MoCl_4(THF)_2]$ itself was also found to be intrinsically unstable; remarkably, this substrate converts into a crystalline material, in which the newly formed Mo(III) and Mo(V) products cohabitate the same unit cell.

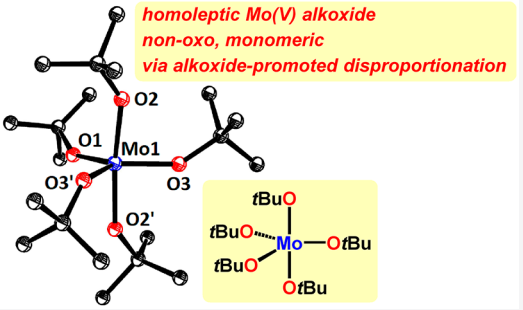

INTRODUCTION

Any systematic exploration of the prodigiously rich (bio)-inorganic, organometallic, organic, catalysis, and material chemistry of molybdenum has to cope with a surprising dearth of practical entry points. $MoCl_5$ is one of them, because this compound is available in bulk quantities at fairly low cost.[1] In solid form, $MoCl_5$ is manageable,[2] despite the rather aggressive chemical character that it draws from the combination of strong Lewis acidity, exceptional oxophilicity, and a pronounced oxidizing power; moreover, $MoCl_5$ is an effective chloride and/or chlorine source. Actually, only few of the commonly used solvents are inert toward $MoCl_5$: benzene and related aromatic hydrocarbons succumb to oligomerization and/or chlorination;[3] ethereal solvents face rapid cleavage with concomitant formation of oxo-molybdenum species such as **2** (THF, dioxanes, hexamethyldisiloxane) (Scheme 1) and/or serve as single electron reducing agents, entailing the release of Cl_2 (Me_2O, DME);[4−7] acetonitrile also leads to reduction with formation of $[MoCl_4(MeCN)_2]$ and chlorinated acetonitrile byproducts.[8] These examples highlight the vigorous reactivity of $MoCl_5$, which can be intentionally used for synthetic purposes, such as the oxidative coupling of (electron-rich) arenes or the formation of esters by catalytic acylative ether cleavage.[7,9]

Ordinary alcohols do not withstand this powerful oxidant and strong Lewis acid either: even primary alcohols R−OH are readily converted into the corresponding alkyl chlorides R−Cl

Scheme 1. Prototypical Reactivity of $MoCl_5$ towards Ethers, Alcohols, and Alkoxides

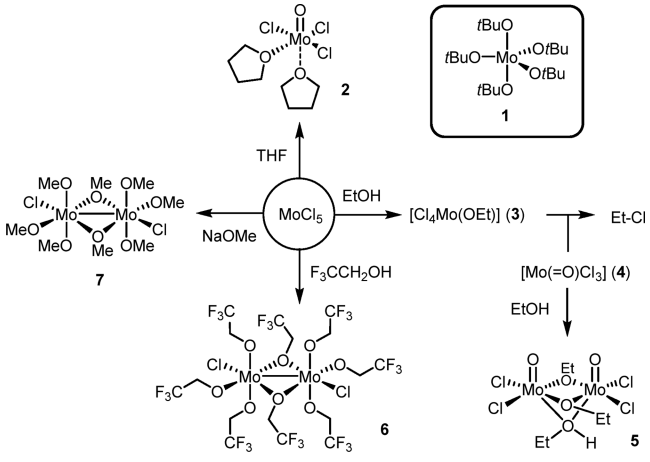

Received: July 1, 2020
Published: August 27, 2020

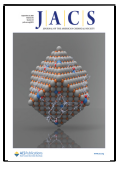

ACS Publications

© 2020 American Chemical Society

https://dx.doi.org/10.1021/jacs.0c07073
J. Am. Chem. Soc. 2020, 142, 16392−16402

(Scheme 1). The reaction is thought to proceed by partial ligand exchange with formation of transient Mo(V) alkoxides (*e.g.*, **3**) followed by rupture of a MoO−R bond; the resulting oxo-molybdenum complexes of type $[O{=}MoCl_3]$ (**4**) dimerize and can lead to adducts such as **5** or even complex polynuclear arrays.[10−13] The ease of formation of the [Mo═O] group manifest in these examples is a hallmark of (high-valent) molybdenum chemistry;[10,14,15] this prevalent functionality dominates the field and plays a pivotal role in biological and industrial catalysis alike.[16,17] Only highly fluorinated alcohols were found to subsist to such degradation: trifluoroethanol, for example, on treatment with $MoCl_5$, affords the stable heteroleptic complex **6**.[18,19] The fact that even the electron-poor O atom of trifluoroethoxide serves as a bridging ligand highlights the very strong bias for dimerization, which is yet another characteristic trait of the coordination chemistry of molybdenum. A closely related binuclear molybdenum(V) alkoxide **7** was prepared by salt metathesis between $MoCl_5$ and NaOMe, but complete ligand exchange could not be accomplished either.[20,21] Analogous reactions with electron-rich alkoxides are unlikely in view of the ease of reduction of $MoCl_5$ even by much milder agents;[22] in any case, no follow-up investigation describing the preparation of analogues of **7** has been published.

It is against this backdrop that the isolation and full characterization of $[Mo(OtBu)_5]$ (**1**) must be seen: even oxo-free alkoxides of Mo(V) with a *mixed* ligand sphere, such as **6** and **7**, are exceedingly rare chemical entities, but homoleptic alkoxides of Mo(V) are elusive and may perhaps even be deemed inaccessible. It is therefore perplexing that complex **1** as the first incarnation of this previously unknown class of compounds carries *tertiary* alkyl residues on all oxygen atoms: *a priori*, these ligands are particularly prone to [Mo═O] formation, independent of whether the actual O−C bond cleavage proceeds in a heterolytic or homolytic manner with release of a stabilized tertiary carbocation or tertiary radical, respectively;[7,23] most notably, the clean and efficient radical breakdown of *tert*-butoxide at a Mo(V) center has been explicitly mentioned in the literature.[24] The fact that **1** is monomeric even in the solid state is equally striking if one considers that a d^1 electron count is potentially conducive to metal−metal bonding.[25,26] Moreover, the sheer size of a *t*BuO group certainly does not exempt it from serving as a bridging ligand;[27] in general, the formation of μ-bridged dimers (oligomers) is so favorable that even very poorly donating fluorinated alkoxides do not get away (*cf.* **6**). Finally, the synthesis of **1** by disproportionation tells fundamental lessons about the meta-stability of low-valent molybdenum complexes in general and, in doing so, casts doubts on previous reports claiming the isolation of putative *tetra*-valent $[Mo(OtBu)_4]$.[28,29]

RESULTS AND DISCUSSION

Preparation and Crystallographic Characterization. For their high activity and excellent functional group tolerance, molybdenum alkylidynes of the general type $[(R^1O)_3Mo{\equiv}CR^2]$ arguably define the state-of-the-art in alkyne metathesis.[30−32] Several independent entries into this privileged class of organometallic catalysts have been developed over the years.[33−39] One of them employs $Mo[N(t\text{-}Bu)(Ar)]_3$[40] derived from $[MoCl_3(THF)_3]$, which in turn is formed by stepwise reduction of $MoCl_5$ with MeCN to give $[MoCl_4(MeCN)_2]$, followed by ligand exchange and further reduction of the resulting complex $[MoCl_4(THF)_2]$ with coarse tin.[8,41] During a reinvestigation of this somewhat tedious prelude to the actual catalyst formation,[34,35] we made the serendipitous discovery that treatment of $[MoCl_4(THF)_2]$ with MO*t*Bu (M = Na, Li; 3 equiv) in toluene at −35 °C delivers a mixture of the well-known diamagnetic dinuclear Mo(III) complex $[(tBuO)_3Mo{\equiv}Mo(OtBu)_3]$ (**8**)[42−44] and a new, green, highly air-sensitive and paramagnetic species, which was isolated by taking advantage of its high solubility in pentane; purification of the crude product by sublimation in high vacuum (23 °C, 10^{-7} mbar) furnished complex **1** in 30% yield (Scheme 2). It is

Scheme 2. Alkoxide-Promoted Disproportionation of Mo(IV)

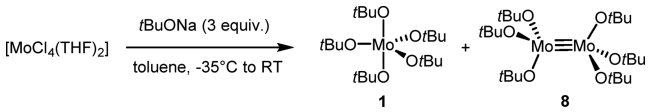

emphasized that formation of **1** in appreciable amounts was observed only under the specified conditions: changing the stoichiometry of the reagents and/or the solvent (THF, *n*-pentane) resulted in lower yields (see the Supporting Information).

Compound **1** is well-soluble in *n*-pentane, benzene, toluene, and CH_2Cl_2 but rapidly decomposes in MeCN at room temperature; it also degrades in $[D_8]$toluene when the solution is warmed to ≥50 °C.[45] Although the high sensitivity rendered elemental analysis challenging, the obtained data matched those calculated for $[Mo(OtBu)_5]$ reasonably well (Anal. Calcd for $C_{20}H_{45}O_5Mo$: C 52.05, H 9.83, Mo 20.79. Found: C 52.33, H 10.01, Mo 20.58). The NMR spectroscopic fingerprint of this paramagnetic species (broad signals in C_6D_6 at δ_H = 7.43 ppm and δ_C = 54.9, 30.3 ppm) is also in accord with the proposed homoleptic structure. This assignment was confirmed when single crystals suitable for X-ray diffraction were obtained from a saturated solution in *n*-pentane at −35 °C.

The unit cell contains two independent molecules, which differ from each other only in conformational detail [for details, see the Supporting Information (SI)].[46] As can be seen from Figure 1, the coordination geometry about the Mo center can be described as approximately trigonal bipyramidal, although notable deviations from the idealized structure are on record: specifically, the O2−Mo1−O2′ angle is only 169.1(5)° rather than 180°, and the angles between the O atoms forming the equatorial plane are uneven and irregular [O1−Mo1−O3, 122.7(5)°; O1−Mo1−O3′, 112.3(5)°; O3−Mo1−O3′, 124.5(5)°]. The Mo1−O2 distance [1.924(5) Å] is distinctly longer than the Mo−O bonds in the equatorial plane [Mo1−O1, 1.875(11) Å; Mo1−O3, 1.857(5) Å]. As will be discussed in detail below, the overall distorted structure of **1** results from a symmetry-lowering Jahn−Teller distortion of the nuclear framework, befitting this d^1 complex (see below).[47]

The fairly clean formation of **1** by disproportionation of $[MoCl_4(THF)_2]$ in the presence of NaO*t*Bu at low temperature was unexpected in view of two earlier literature reports. Specifically, it had been reported that treatment of $[MoCl_4(THF)_2]$ with LiO*t*Bu in THF/hexane entails simple ligand exchange; a workup with CH_2Cl_2 followed by recrystallization from cold *n*-pentane supposedly gave $[Mo(OtBu)_4]$ in 25% yield.[29] This assignment, however, had been

https://dx.doi.org/10.1021/jacs.0c07073
J. Am. Chem. Soc. 2020, 142, 16392−16402

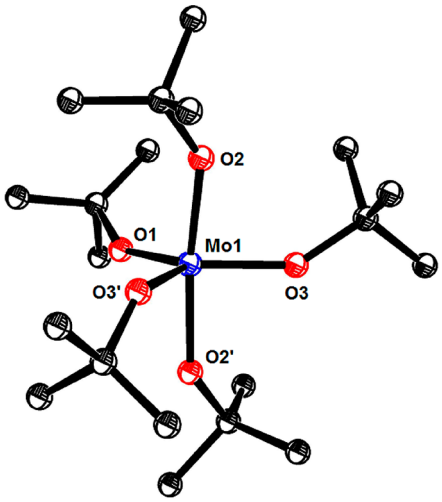

Figure 1. Structure of $[Mo(OtBu)_5]$ (**1**) in the solid state; only one of the two independent molecules in the unit cell is depicted, and H atoms are omitted for clarity.

based on a rather rudimentary characterization by elemental analysis and the fact that a single resonance in the ^{1}H NMR spectra was observed; the compound was reported to be EPR-silent.[29] In our hands, treatment of $[MoCl_4(THF)_2]$ with either NaO*t*Bu or LiO*t*Bu invariably resulted in disproportionation with formation of **8**[48] and **1**; the latter is EPR-active (see below). Unfortunately, the paucity of data reported for $[Mo(OtBu)_4]$ precludes a detailed comparison with **1** and an accurate assessment. We cannot exclude that $[Mo(OtBu)_4]$ had previously been formed by ligand exchange,[29] yet we are also unable to confirm it, despite considerable experimentation.

A second report describes $[Mo(OtBu)_4]$ as a thermally unstable green-brown solid material formed on reaction of $[Mo(NMe_2)_4]$, with *t*BuOH.[28] Its characterization was based upon elemental analysis, IR, and mass spectrometry: it is stunning, however, that the peak in the reported mass spectrum with the highest m/z 461 actually fits to $[Mo(OtBu)_5]^+$,[49] although the observed base-peak at m/z 388 matches the mass of $[Mo(OtBu)_4]^+$.[28] The reported IR data have not been analyzed in any detail and therefore do not allow one to make a final judgment; we note that the reported bands are close to those observed for **1** (see below). In consideration thereof, we tried to reproduce this literature route (Scheme 3). Although it cannot be rigorously excluded that $[Mo(OtBu)_4]$ is present in the crude mixture, the only complexes that we were able to isolate in pure form in several independent runs were, once again, $[Mo(OtBu)_5]$ (**1**) and the new dinuclear species **9**. From the structure in the solid state it is apparent that **9** contains a bridging amide and a bridging oxo-ligand; moreover, a molecule of Me_2NH released upon reaction of $[Mo(NMe_2)_4]$ with *t*BuOH now serves as a donor ligand to one the Mo centers (Figure 2). The short Mo1−Mo2 distance [2.486(3) Å] speaks for a metal−metal bonding interaction

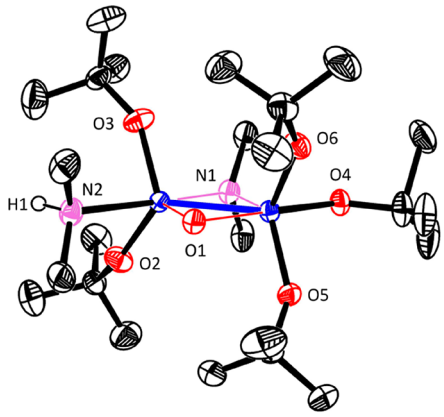

Figure 2. Structure of complex **9** in the solid state; hydrogen atoms (except for the NH atom) and the disorder of one of the *tert*-butyl groups over two positions are not shown for clarity

within the core of this paramagnetic species.[50] The question as to how this peculiar product is formed has to remain open at this point. The fact that the μ-oxo atom can only derive from a *t*BuO precursor ligand could imply an oxidative cleavage mechanism, which might transform a transient dinuclear Mo(III) precursor as the expected low-valent product of the actual disproportionation reaction into the ultimately isolated complex **9**.

Collectively, these results suggest that alkoxide ligands favor the disproportionation of Mo(IV), even though a discrete and well-characterized homoleptic Mo(IV) enolate complex is known that has been made from $[MoCl_4(THF)_2]$ by ligand exchange with the corresponding bulky alkali-metal enolate.[51] $[MoCl_4(THF)_2]$ itself also shows the propensity to disproportionate, although more latently.[52] This complex had previously been recognized as unstable under nitrogen atmosphere, but the decomposition products had not been identified.[8b] When a solution of $[MoCl_4(THF)_2]$ in dichloromethane was kept at ambient temperature for ≥4 d, a solid material started to precipitate that is composed of a 1:1 mixture of the oxo-species **10**, crystallized with one THF and one adventitious water ligand,[53] and the known dinuclear complex **11** (Scheme 4).[54]

Scheme 4. Disproportionation of Mo(IV) in the Absence of Alkoxides

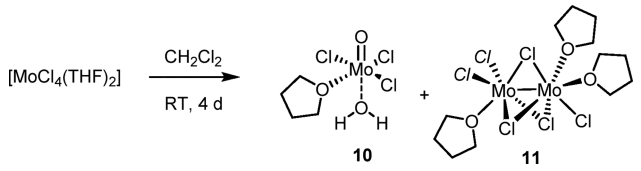

The coexistence of these Mo(V) and Mo(III) complexes in a single unit cell is unprecedented (Figure 3);[55] it provides compelling evidence for the notion that Mo(IV) is inherently

Scheme 3. Literature-Inspired Control Experiment

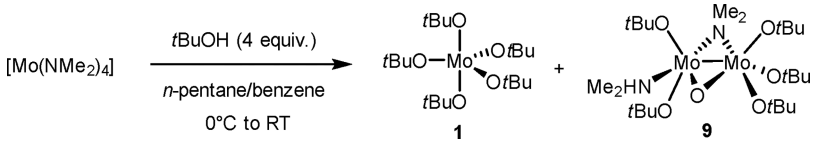

https://dx.doi.org/10.1021/jacs.0c07073
J. Am. Chem. Soc. 2020, 142, 16392−16402

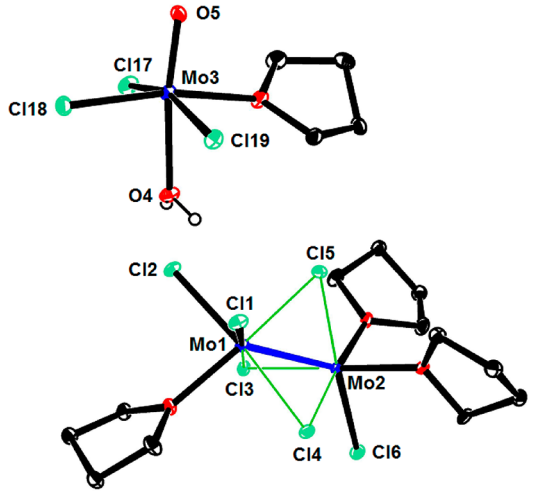

Figure 3. Structure of cocrystallized **10** and **11**; hydrogen atoms are omitted except for those of the adventitious water molecule completing the ligand sphere of the oxo-complex **10**.

unstable, although the rate of disproportionation is dependent on the particular ligand sphere and the reaction conditions.

In any case, $[Mo(OtBu)_5]$ (**1**) is the prototype of a new class of high-valent molybdenum complexes, the existence of which is rather counterintuitive; such monomeric, homoleptic, five-coordinate, all-oxygen-ligated but non-oxo $4d^1$ Mo(V) species were previously unknown. For this unique status, it was deemed appropriate to scrutinize the structure and bonding of this new chemical entity in more detail by a combined spectroscopic and theoretical approach.

Computational Study: Structure. The geometry-optimized structure **1a** of $[Mo(OtBu)_5]$ (**1**) starting from the crystal structure geometry is shown in Figure 4. The computed

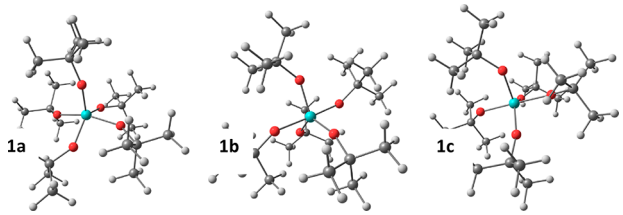

Figure 4. Structures of the three lowest minima on the potential energy surface, found by geometry optimizations from different starting structures. Structure **1a** was found by geometry-optimizing the crystal structure; this structure is closest to an idealized square pyramid. Structures **1b** and **1c** show a more trigonal bipyramidal structure of the MoO_5 core. The structures additionally differ in the relative orientations of the *t*Bu groups. All three structures are within 3 kcal/mol of each other, with **1b** being lowest in energy. Cartesian coordinates are provided in the Supporting Information.

structure (see the Supporting Information for computational details) is intermediate between square pyramidal and trigonal bipyramidal, thus rendering all O atoms inequivalent. The distortion from trigonal bipyramidal and square pyramidal can be quantified by a Berry pseudorotation, where the O3−Mo−O1 angle has decreased from 180° (square pyramidal limit) to 135.7°. Since the complex is homoleptic, multiple minima likely exist on the potential energy surface;[47] as such, the system is Jahn−Teller-active.

A comparison between the crystal structure and the optimized geometry based on the crystal structure shows a good agreement (Table 1). The axial direction of the trigonal

Table 1. Selected Bond Distances (Å) and angles (deg) of Complex 1 Compared to Model 1a

distance			angle		
	exp	DFT		exp	DFT
Mo−O1	1.875	1.918	O2−Mo−O2′	169.1	160.6
Mo−O2	1.923	1.937			
Mo−O2′	1.923	1.946	O1−Mo−O3	122.7	135.7
Mo−O3	1.857	1.923	O1−Mo−O3′	112.3	111.3
Mo−O3′	1.857	1.824	O3−Mo−O3′	124.5	113.0

bipyramid is given by the O2−Mo and/or Mo−O2′ direction (O2−Mo−O2′ = 160.6°). The low symmetry of the molecule also leads to an inequivalence of the *x* and *y* directions. This geometrical aspect is indeed reflected, for example, in the observation of a rhombic EPR spectra (see below).

In addition, in an effort to explore the potential energy surface in more depth, additional geometry optimizations were performed with modified starting structures, by rotating the *t*Bu groups about the Mo−O direction in various permutations. While some calculations ended up converging to identical minima, a range of stable, slightly different conformations have indeed been found, indicative of a potential energy surface with multiple close-lying minima.

Figure 4 features two additional optimized structures (**1b**, **1c**) that clearly show structural differences. The geometry optimization starting from the crystal structure **1a** gave rise to the most square pyramidal structure. The middle and rightmost structures are significantly more trigonal bipyramidal. Structure **1b** turned out to be the most stable structure *in vacuo*. However, the energy difference with respect to **1a** and **1c** is only 2.5 and 1.6 kcal/mol, respectively, which is well within the accuracy of the employed DFT methodology; as such, the observation that structure **1b** is most stable with the present choice of functional, method, and basis set should not be overinterpreted. Rather, these calculations should be viewed of as an *in silico* confirmation of the presence of multiple, closely related local minima that differ by rotation of the *t*Bu groups about the respective Mo−O bond directions.

Given the small energy differences of the structures in Figure 4, it is by all means conceivable that local minima become thermally populated at elevated temperature and depopulated at low cryogenic temperature, which is in-line with the observed temperature dependence of the EPR signal (*vide infra*). Moreover, when the *t*Bu groups rotate about the Mo−O direction, the hybridization of the oxygen orbitals, and thus the covalency of the Mo−O bonds, is expected to be altered, resulting in changed Mo−O covalencies. This in turn may lead to a continuous or discrete distribution in spectroscopic parameters like EPR *g*-values and chemical shifts, in the ligand field splitting parameters and transition energies observable in MCD, and even in the powder diffraction pattern.

Powder Diffraction. In order to investigate possible structural heterogeneities experimentally, we have recorded powder diffraction patterns of several batches. The results, shown in Figure 5, indeed confirm that a discrete structural heterogeneity may be present: whereas the measured pattern for the batch shown in Figure 5b matches the expected pattern calculated from the crystal structure reasonably well (Figure

https://dx.doi.org/10.1021/jacs.0c07073
J. Am. Chem. Soc. 2020, 142, 16392−16402

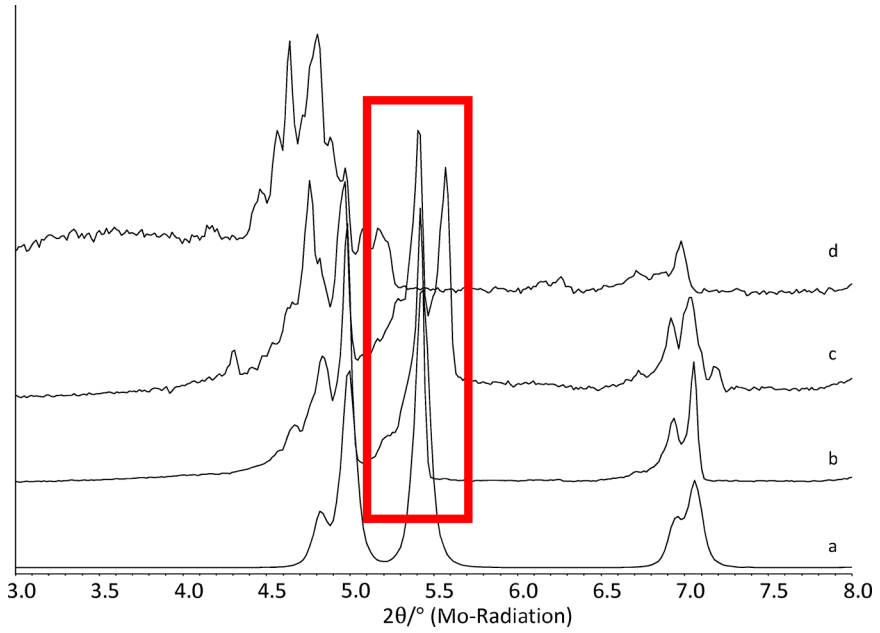

Figure 5. (a) Theoretical diffraction pattern of complex $[Mo(OtBu)_5]$ (**1**) obtained by single-crystal data. (b) Second batch of $[Mo(OtBu)_5]$ (**1**). (c) First batch of $[Mo(OtBu)_5]$ (**1**). (d) Complex $[Mo_2(OtBu)_6]$ (**8**).

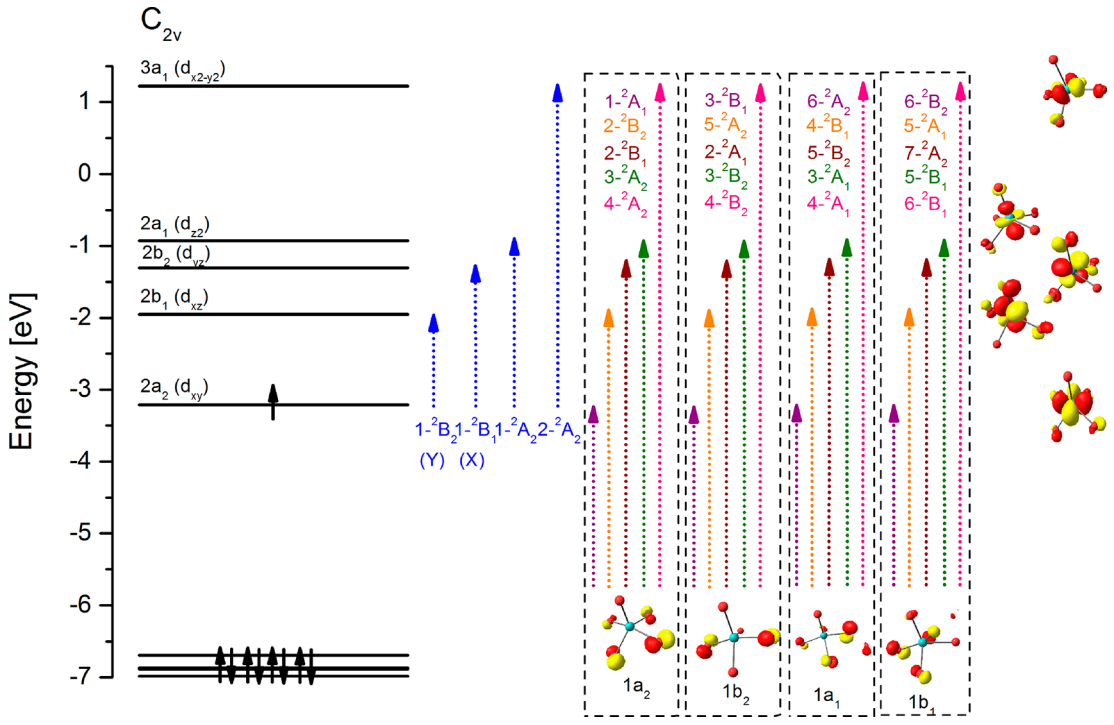

Figure 6. Molecular orbital scheme (quasi-restricted orbitals) for the 4d manifold of $[Mo(OtBu)_5]$ represented by the geometry-optimized crystal structure **1a**. Also included are four representative oxygen-based doubly occupied orbitals (at about −6.8 eV). Since the orbital structure largely corresponds to that of a square pyramid, the molecular *z*-axis is chosen as parallel to the Mo−O3′ direction and the *x*-axis as along the O2−O2′ direction. Symmetry labels under approximate C_{2v} symmetry were added accordingly for the orbitals and for the transitions; the *t*Bu groups are omitted for clarity. Upon consideration of the ligand character, the low-lying *y*-polarized $^2B_2$ and *x*-polarized $^2B_1$ d−d transitions (blue) are expected to gain oscillator strength owing to an overlap of the ligand part of the donor orbital with the metal part of the acceptor orbital, leading to a symmetry-allowed, nonzero transition dipole moment upon admixture of ligand character into the orbital. Electronic excitations from the oxygen-centered doubly occupied orbitals with approximate C_{2v} symmetry labels are included in the dashed boxes.

5a), the pattern of a second batch in Figure 5c shows a splitting of the band at 5.5°. Moreover, this sample also seems to contain some dimer, $[Mo_2(OtBu)_6]$. While the powder pattern clearly confirms the presence of two discrete conformers, the measured data does not contain enough information to allow a confident identification of the second structure of the monomer.

Electronic Structure. In spite of the significant Berry rotation of the optimized crystal structure **1a**, the computed d-orbital scheme of **1a** shown in Figure 6 closely resembles that

https://dx.doi.org/10.1021/jacs.0c07073
J. Am. Chem. Soc. 2020, 142, 16392−16402

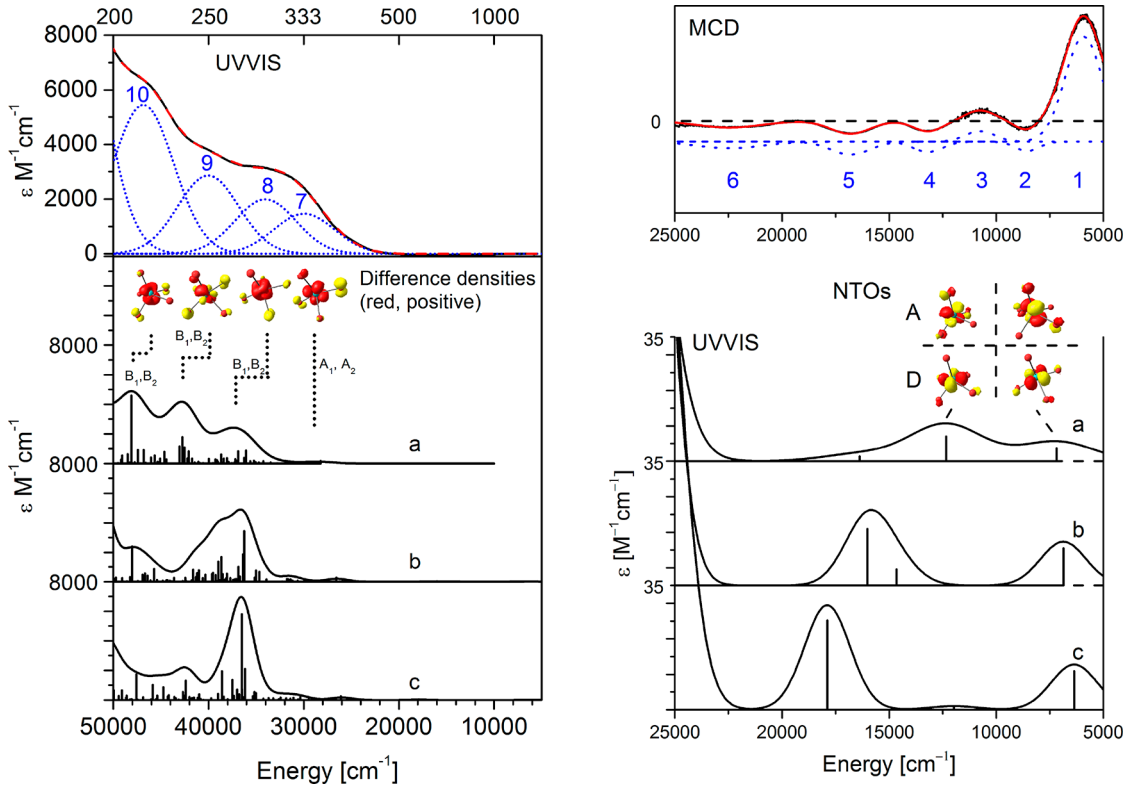

Figure 7. UV/vis (T = 296 K, left) and MCD (T = 2 K, B = 10 T, right) spectra of **1** (black) and their simulations (red) and Gaussian deconvolution (blue). The UV/vis sample was a pentane solution, whereas MCD was obtained from a mull. The bottom panels show in addition calculated UV/vis spectra (bottom) as obtained for the structural models **a**, **b**, and **c** with sticks representing the number of possible transitions. Also included are the natural transition orbitals for the lowest two calculated d−d transitions and the difference densities (red, positive) for bands 7−10, structure **1a**.

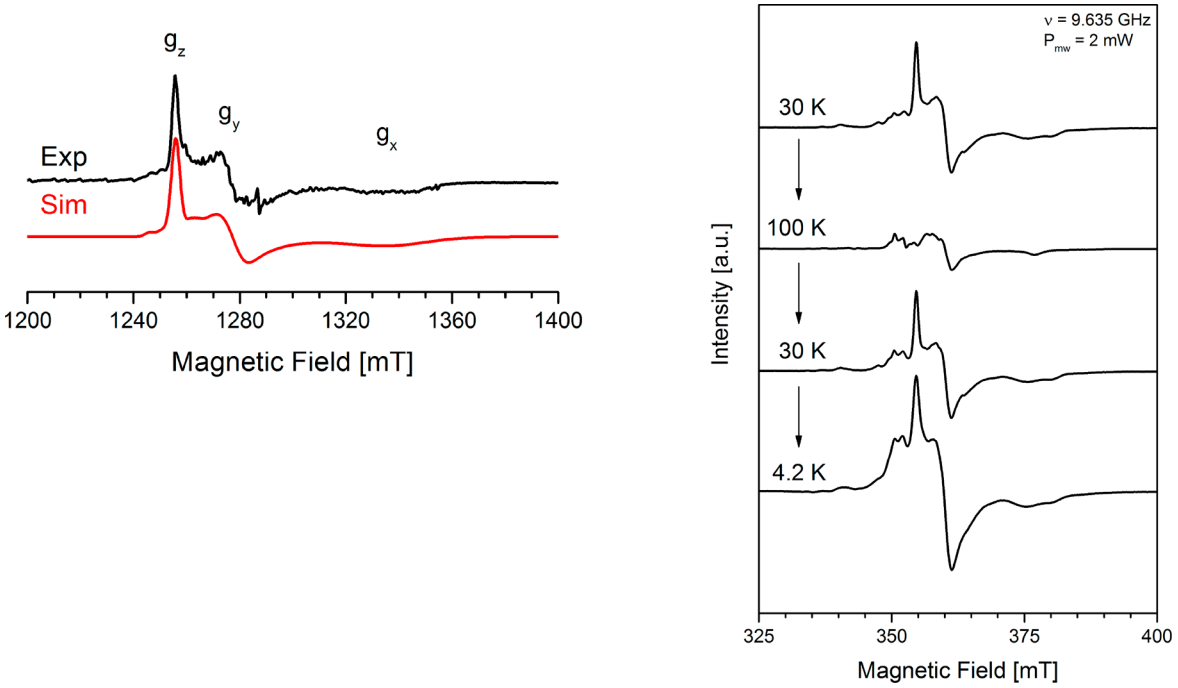

Figure 8. (Left) Continuous wave Q-band EPR spectrum of [Mo(O*t*Bu)$_5$] (**1**) in *n*-pentane and a simulation. Experimental conditions: T = 20 K, microwave frequency 34.053 GHz, microwave power 0.1 mW, modulation amplitude 0.78 mT. The *g*-values extracted from the simulation amount to 1.818, 1.903, and 1.936. The fitted Mo(V) hyperfine coupling constants amount to 145, 10, and 61 MHz. (Right) Temperature cycle from 30 to 100 K back to 30 K and to 4.2 K of one sample, recorded at the X-band. Conditions: microwave frequency 9.635 GHz, microwave power 2 mW.

https://dx.doi.org/10.1021/jacs.0c07073
J. Am. Chem. Soc. 2020, 142, 16392−16402

expected for a square pyramidal coordination geometry. The unpaired electron is located in the nonbonding d_{xy} orbital. The other orbitals are destabilized owing to the metal−ligand interactions: specifically, the SOMO is followed by the d_{xz}/d_{yz} pair, the degeneracy of which has been lifted by the Jahn−Teller distortion. Next comes the d_{z^2} orbital and finally, as the most destabilized orbital, $d_{x^2-y^2}$. The symmetry labels of the orbitals under approximate C_{2v} symmetry (vide infra) are included in Figure 6. Inspection of the doubly occupied orbital structure reveals a plethora of "nonbonding" linear combinations of oxygen-centered orbitals (the first four are included in Figure 6) that do not directly overlap with the Mo 4d orbitals owing to symmetry. This set of orbitals occurs at about 3.5 eV (28 000 cm^{-1}) in energy below the SOMO. The first oxygen-based orbital with bonding character to Mo occurs even lower, at −8.50 eV, in which the oxygen orbitals are π-bonding to the $4d_{xy}$ orbital (not shown in the figure). While it is in principle possible to induce a z-polarized $^2A_1$ charge-transfer transition from this orbital into the SOMO, this electronic transition is expected at an energy above 40 000 cm^{-1}, where it would be difficult to detect. A comparison of the electronic differences in terms of ligand field splittings of complexes **1a**−**1c** is given in the Supporting Information.

UV/Vis and MCD Spectroscopy. The UV/vis spectrum displays a broad and relatively featureless absorption in the blue part of the spectrum (Figure 7, left). It could be well-deconvoluted with four Gaussians of width 6400 cm^{-1}, centered at 29 950, 34 030, 40 035, and 46 850 cm^{-1}. In order to investigate whether d−d transitions are present in the infrared region, we recorded an MCD spectrum on a concentrated sample, which is surprisingly rich in structure and displays a multitude of bands in the infrared region (Figure 7, right). A particularly strong band is present at about 6000 cm^{-1}, indicating the presence of multiple d−d transitions that are not observed in the UV/vis spectrum. The MCD spectrum has been fitted with six Gaussians centered at 5935, 8616, 11 100, 12 808, 16 804, and 22 499 cm^{-1}. The observation of six transitions in the MCD spectrum below 23 000 cm^{-1} is already remarkable for a $4d^1$ system in itself, since only a maximum of four d−d transitions can occur; on the basis of our calculations, we do not expect more than three d−d transitions below 20 000 cm^{-1} [*cf.* Figure S9 (SI) and *vide infra*]. Thus, this observation provides additional evidence for the coexistence of several conformers under the experimental conditions. Attempts to address the structural heterogeneity by additional MCD experiments of deposited and smeared-out monocrystalline material were not successful due to scattering, as were experiments with frozen solutions, since *n*-pentane and toluene or mixtures thereof produced a poor glass at low temperature. The calculations shown in Figure 7 will be discussed in the Theoretical Spectroscopy section.

EPR Spectroscopy. The Q-band continuous wave (cw) EPR spectrum (Figure 8) has been well-fitted by using a minimalistic spin Hamiltonian that included the three g-values and the Mo hyperfine coupling constants, as well as three line width parameters. The fitted g-values amount to 1.818, 1.903, and 1.936. The observed rhombicity of the g-tensor provides direct confirmation of the symmetry-lowering of $[Mo(OtBu)_5]$ (**1**) as compared to the structure of this complex in the solid state. It is worth noting that the g_x feature of the EPR spectrum shows a splitting in two poorly resolved bands. A comparison of spectra recorded at the X-band and Q-band (Supporting Information) indicates that the two bands are not caused by hyperfine splitting and must stem from slightly different conformers present in frozen solution, with possibly slightly altered orientation of the *t*Bu groups and thereby slightly changed Mo−O covalencies and thus g-values.

Being aware of possible structural heterogeneity, we investigated the EPR spectrum as a function of temperature. The temperature dependence in Figure 8 (right) measured at the X-band displays a drastic change of the spectrum upon raising the temperature from 30 to 100 K, in the form of the disappearance of the intense signal at 360 mT and the merging together of the g_z feature at 380 mT. The change is completely reversible, as subsequent cooling of the sample back to 30 K recovered the original signal. The spectrum at 4.2 K is essentially identical to the one at 30 K. The change in shape of the signal with temperature and, in particular, the presence of a split g_z signal at low temperature provide a rather strong experimental indication of the presence of two conformers corresponding to local minima of the potential energy surface of the Jahn−Teller-active molecule, the thermal populations of which change.

Theoretical Spectroscopy. In order to interpret the recorded spectra, a detailed comparison with quantum chemical calculations is necessary. A particular problem occurs in interpreting the six bands in the MCD spectrum (Figure 7). First, the AILFT calculation (Figure S9, SI) that included the five 4d orbitals and one electron features only three d−d transitions below 20 000 cm^{-1}. The natural transition orbitals for the lowest two transitions are included in Figure 7. These are the 1-^2B_2 and 1-^2B_1 transitions featuring the d_{xy} orbital as the donor orbital and the d_{xz}, d_{yz} pair as the acceptor orbitals. Out of all four d−d transitions these two are expected to have the largest oscillator strength. The oxygen-centered nonbonding orbitals were not included in the CAS calculation, because they are located more than 3.5 eV below the SOMO.

The seemingly doubled number of bands in the MCD spectrum, in addition to the observed splitting of the g_z feature in the EPR spectrum (Figure 8) and the splitting observed at 5.5° for one of the batches in the powder diffraction pattern (Figure 5c), is compatible with the presence of two conformers with perhaps slightly changed orientations of the O*t*Bu groups and, concomitantly, slightly changed Mo−O covalencies. This is additionally confirmed by the calculations of the electronic spectrum, where structures **1a**, **1b**, and **1c** each display two bands in the near-infrared region at different positions (Figure 7, bottom, right), which is a direct consequence of the slightly changed ligand field splitting of the conformers (Figure S9, SI). While a definite assignment of the bands in the MCD spectrum seems presently not feasible owing to the Jahn−Teller-induced heterogeneity, the mere observation of these bands in the near-IR region shows unambiguously that the molecular species does not feature an oxo-ligand. An oxo-ligand, in turn, would lead to an MCD spectrum where the lowest d−d transition would be significantly higher in energy, *e.g.*, 20 000 cm^{-1} in $[Mo(O)Cl_3\cdot(dppe)])$[56] or larger than 23 000 cm^{-1} in a derived *in silico* $[MoO(OtBu)_4]^-$ complex contained in the Supporting Information (Figure S7).

Analysis of the g-values in terms of ligand field theory (see the Supporting Information) yielded good agreement with experiment. However, a confident, detailed assignment of all low-energy MCD bands could not be achieved. The calculated g-values for structure **1a** amount to 1.87, 1.94, and 1.95, in reasonable agreement with experiment, whereby in particular the middle g-shift is calculated slightly too small. The

https://dx.doi.org/10.1021/jacs.0c07073
J. Am. Chem. Soc. 2020, 142, 16392−16402

calculated Löwdin spin population at Mo amounted to 85%, and the calculation was largely spin-uncontaminated ($\langle S^2 \rangle$ = 0.754). The more-trigonal geometries **1b** and **1c** found on the potential energy surface gave rise to slightly different *g*-values, typically changed by about 0.02 (Table S7, SI).

It is instructive to investigate the observed splitting of the least-shifted *g*-value, g_z. In perturbation theory, the g_z shift in structure **1a** arises from the matrix elements of spin−orbit coupling and the orbit−Zeeman interaction between the $(xy)^1$ ground state and the $(x^2-y^2)^1$ excited state [$3a_1$, $\Delta E(xy,x^2-y^2)$ = 34 540 cm^{-1}]. In structures **1b** and **1c**, the least-shifted *g*-value occurs between the $(xz)^1$ ground state and contributions of both the $(z^2)^1$ (1a′) and the $(x^2-y^2)^1$ (1e″) excited states. The excitation energy of the 1e″ contribution changes from 17 667 to 19 883 cm^{-1} upon going from **1b** to **1c** (*cf.* Figure S9, SI), *i.e.*, a change of 12.5%, which would lead to a change of the *g*-values of up to 0.008, compatible with experiments and thus providing yet another confirmation of the Jahn−Teller heterogeneity between the C_{2v} and C_{3h} structures.

Subsequently, a TDDFT calculation has been performed in order to assign bands 7−10 in the UV/vis spectrum shown in Figure 7. The agreement between experiment and theory is good for structure **1a**, providing additional confidence that the chosen model accurately mimics the actual structure of [Mo(O*t*Bu)$_5$] (**1**). Structures **1b** and **1c**, although essentially equal in energy to structure **1a**, seem to provide a less accurate description of the UV/vis spectrum. The plethora of individual transitions (depicted as sticks) included in the diagram gives information that a large number of transitions contribute to the Gaussians used in the deconvolution. As already noted, the large number of transitions originates from the presence of a large number of ligand-centered orbitals, mainly with oxygen character, that are located about 3.5 eV below the SOMO. Difference densities for representative sticks are included in Figure 7. Although the relative phases of the oxygen orbitals inhibit admixture of Mo(4d) character, all of these orbitals principally contribute to the rich manifold of excited states that are all formally of oxygen-to-molybdenum charge-transfer character. The more intense transitions involve the B_1 and B_2 transitions of the $1a_2$, $1b_2$, $1a_1$, and $1b_1$ orbitals as donor orbitals (*cf.* Figure 6).

Most convincingly, the calculated IR spectra for all three model structures included in Figure S11 (SI) reproduce virtually all bands observed in the experimental spectrum very nicely and hence allows for their assignment (see the Supporting Information).

Overall, we conclude that despite the observed complications owing to temperature-dependent structural heterogeneity, generally excellent agreement between experiment and theory is found for all spectroscopic methods employed in this study. This provides confidence in the model structures used in the calculations. The calculated geometric and electronic structure therefore accurately represents the so far unique homoleptic Mo(V) alkoxide [Mo(O*t*Bu)$_5$] (**1**), including the symmetry-lowering as a result of Berry rotation.

CONCLUSION

The chemistry of Mo(V) is dominated by oxo-complexes, which are readily formed by formal oxygen atom abstraction even from substrates as stable as ethers, phosphine oxides, sulfoxides, and, most commonly, alcohols. Due to the proclivity to form and maintain [Mo═O] groups, Mo(V)-alkoxides devoid of at least one additional oxo-ligand in general are exceedingly rare, and homoleptic representatives were entirely unknown prior to the present study. It is now shown that disproportionation of Mo(IV) provides access to this previously elusive class of compounds under notably mild conditions. The first embodiment is [Mo(O*t*Bu)$_5$] (**1**). This compound is a monomeric entity with a Jahn−Teller-distorted trigonal bipyramidal structure in the solid state but is subject to facile symmetry-lowering Berry pseudorotation in solution. The geometric and electronic structures of this unique complex are accurately described by DFT, which was calibrated against experimental spectra (IR, UV/vis, MCD, EPR).[57]

Indirect evidence suggests that alkoxide ligands render the disproportionation reaction of Mo(IV), leading to the formation of [Mo(O*t*Bu)$_5$], remarkably facile, even though [$MoCl_4(THF)_2$] was also found to be intrinsically unstable toward decay into Mo(III) and Mo(V) in CH_2Cl_2 solution at ambient temperature. The question whether the increased reaction rate in the presence of *tert*-butoxide has to do with the formation of the dinuclear complex [(*t*BuO)$_3$Mo≡Mo(O*t*Bu)$_3$] as a particularly favorable low-valent product of the disproportionation process or if stabilization of [Mo(O*t*Bu)$_5$] itself by dispersive forces within the ligand sphere[58,59] plays any significant role will be the subject of future studies.

ASSOCIATED CONTENT

Supporting Information

The Supporting Information is available free of charge at https://pubs.acs.org/doi/10.1021/jacs.0c07073.

An experimental part including procedures; characterization data; supporting crystallographic information; EPR experiments in X-, Q-, and W-bands; NMR spectroscopy; infrared spectroscopy; a computational part including methodological details and a comparison of the ligand field splitting of structures **1a**−**1c** and comparison to an *in silico* Mo^V−oxo model (PDF)

X-ray crystallographic data for penta-(*tert*-butoxy)-molybdenum(V) in CIF format (CIF)

X-ray crystallographic data for tris(μ_2-chloro)-trichloro-tris(tetrahydrofuran)-di-molybdenum trichloro-oxo-tetrahydrofuran-aqua-molybdenum in CIF format (CIF)

X-ray crystallographic data for (μ_2-dimethylamido)-(dimethylamine)-(μ_2-oxo)-penta(*tert*-butoxy)-di-molybdenum in CIF format (CIF)

AUTHOR INFORMATION

Corresponding Authors

Frank Neese − *Max-Planck-Institut für Kohlenforschung, 45470 Mülheim/Ruhr, Germany;* orcid.org/0000-0003-4691-0547; Email: Neese@kofo.mpg.de

Alois Fürstner − *Max-Planck-Institut für Kohlenforschung, 45470 Mülheim/Ruhr, Germany;* orcid.org/0000-0003-0098-3417; Email: Fuerstner@kofo.mpg.de

Authors

Julius Hillenbrand − *Max-Planck-Institut für Kohlenforschung, 45470 Mülheim/Ruhr, Germany;* orcid.org/0000-0002-2646-1302

Maurice van Gastel − *Max-Planck-Institut für Kohlenforschung, 45470 Mülheim/Ruhr, Germany;* orcid.org/0000-0002-1547-6365

Eckhard Bill − *Max-Planck-Institute for Chemical Energy Conversion, 45470 Mülheim/Ruhr, Germany;* orcid.org/0000-0001-9138-3964

Complete contact information is available at: https://pubs.acs.org/10.1021/jacs.0c07073

Notes

The authors declare no competing financial interest.

■ ACKNOWLEDGMENTS

Generous financial support by the MPG is gratefully acknowledged. We thank Mr. N. Nöthling and Dr. R. Goddard, Mülheim, for solving the X-ray structures; Priv.-Doz. Dr. C. Weidenthaler, J. Ternieden, and P. Unkel, for powder diffraction measurements; Dr. M. Leutzsch, for help with NMR spectroscopy; and the analytical departments of the MPI, for excellent support.

■ REFERENCES

(1) The empirical formula "$MoCl_5$" is used throughout this paper for convenience. Note that $MoCl_5$ is dimeric the solid state but (largely) monomeric in the gas phase; solvent-dependent equilibria between dimer and monomer seem to exist in solution. (a) Schäfer, H.; Schnering, H.-G. V.; Tillack, J.; Kuhnen, F.; Wöhrle, H.; Baumann, H. Neue Untersuchungen über die Chloride des Molybdäns. *Z. Anorg. Allg. Chem.* **1967**, *353*, 281−310. (b) Beck, J.; Wolf, F. Three New Polymorphic Forms of Molybdenum Pentachloride. *Acta Crystallogr., Sect. B: Struct. Sci.* **1997**, *B53*, 895−903. (c) McGuire, M. A.; Pandey, T.; Mu, S.; Parker, D. S. Ferromagnetic Spin-1/2 Dimers with Strong Anisotropy in $MoCl_5$. *Chem. Mater.* **2019**, *31*, 2952−2959.

(2) Black-crystalline $MoCl_5$ is moisture sensitive and should be kept under inert atmosphere; because hydrolysis, which leads to the appearance of a greenish color, is rather slow, the compound can be manipulated in air for short periods of time.

(3) (a) Kovacic, P.; Lange, R. M. Polymerization of Benzene to *p*-Polyphenyl by Molybdenum Pentachloride. *J. Org. Chem.* **1963**, *28*, 968−972. (b) Kovacic, P.; Lange, R. M. Reactions of Molybdenum Pentachloride and Vanadium Tetrachloride with Alkyl- and Halobenzenes. *J. Org. Chem.* **1965**, *30*, 4251−4254.

(4) (a) Marchetti, F.; Pampaloni, G.; Zacchini, S. The reactivity of molybdenum pentachloride with ethers: routes to the synthesis of $Mo^{IV}Cl_4$ adducts, Mo(V) chloro-alkoxides and Mo(V) oxydochloride. *Dalton Trans.* **2013**, *42*, 15226−15234. (b) Hey-Hawkins, E.; von Schnering, H.-G. Synthese und Kristallstruktur von $MoCl_4$(DME)·15-Krone-5 und $MoCl_4$(DME) (DME = 1,2-Dimethoxyethan). *Z. Naturforsch., B: J. Chem. Sci.* **1991**, *46*, 307−314.

(5) (a) Dolci, S.; Marchetti, F.; Pampaloni, G.; Zacchini, S. A systematic study on the activation of simple polyethers by $MoCl_5$ and WCl_6. *Dalton Trans.* **2010**, *39*, 5367−5376. (b) Gibson, V. C.; Kee, T. P.; Shaw, A. The Use of Silylethers and Silylthioethers in Synthesis of Oxohalide and Thiohalide Compounds of Molybdenum and Tungsten. *Polyhedron* **1990**, *9*, 2293−2298.

(6) For the cleavage of THF and the characterization of the resulting molybdenum complex [$MoOCl_3(THF)_2$], see the following: (a) Feenan, K.; Fowles, G. W. A. Reactions of Molybdenum(V) Chloride and Molybdenum(V) Oxotrichloride with Some Oxygen and Sulfur Donor Molecules. *Inorg. Chem.* **1965**, *4*, 310−313. (b) Vitzthumecker, C.; Robinson, F.; Pfitzner, A. Structural characterization of $MoOCl_3(THF)_2$, the pre-reagent for Kauffmann olefination reactions. *Monatsh. Chem.* **2017**, *148*, 629−633.

(7) In the present context, it is particularly relevant to note that it is the *t*Bu−O bond of *t*BuOMe that is selectively cleaved by $MoCl_5$; see the following: (a) Guo, Q.; Miyaji, T.; Gao, G.; Hara, R.; Takahashi, T. Catalytic C-O bond cleavage of ethers using group 5 or 6 metal halide/acid chloride systems. *Chem. Commun.* **2001**, 1018−1019. (b) Guo, Q.; Miyaji, T.; Hara, R.; Shen, B.; Takahashi, T. Group 5 and group 6 metal halides as very efficient catalysts for acylative cleavage of ethers. *Tetrahedron* **2002**, *58*, 7327−7334.

(8) (a) Dilworth, J. R.; Zubieta, J.; et al. Trichlorotris-(tetrahydrofuran)-Molybdenum(III). *Inorg. Synth.* **2007**, *24*, 193−194. (b) Dilworth, J. R.; Richards, R. L.; et al. The Synthesis of Molybdenum and Tungsten Dinitrogen Complexes. *Inorg. Synth.* **2007**, *28*, 33.

(9) (a) Schubert, M.; Waldvogel, S. R. Mo^V Reagents in Organic Synthesis. *Eur. J. Org. Chem.* **2016**, *2016*, 1921−1936. (b) Waldvogel, S. R.; Trosien, S. Oxidative transformations of aryls using molybdenum pentachloride. *Chem. Commun.* **2012**, *48*, 9109−9119.

(10) (a) Garner, C. D.; Charnock, J. M. Molybdenum(III), (IV) and (V). In *Comprehensive Coordination Chemistry*; Wilkinson, G., Gillard, R. D., McCleverty, J. A., Eds.; Pergamon: Oxford, 1987; Vol. *3*, pp 1329−1374. (b) Young, C. G. Molybdenum. In *Comprehensive Coordination Chemistry II*; McCleverty, J. A., Meyer, T. J., Eds.; Pergamon: Oxford, 2003; Vol. *4*, pp 415−527.

(11) (a) Limberg, C.; Parsons, S.; Downs, A. J.; Watkin, D. J. Isolation and Crystal Structure of a Dimeric Oxomolybdenum(V) Complex containing Two Ethoxy Bridges and one Ethanol Bridge. *J. Chem. Soc., Dalton Trans.* **1994**, 1169−1174. (b) Limberg, C.; Downs, A. J.; Blake, A. J.; Parsons, S. Modeling the Formation of Molybdenum Oxides from Alkoxides: Crystal Structures of $[Mo_4O_4Cl_4(\mu^2\text{-}OEt)_4(HOEt)_2(\mu^3\text{-}O)_2]$ and $[PPN]^+[Et_3NH]^+[Cl_2(O)Mo(\mu^2\text{-}O)_2Mo(O)Cl_2]^{2-}$. *Inorg. Chem.* **1996**, *35*, 4439−4448. (c) Limberg, C.; Boese, R.; Schiemenz, B. Intermediates and products of the reaction of $MoCl_5$ with ethanol: crystal structures of $[MoOCl_3(EtOH)]$ and $H[MoOCl_4]\cdot 2EtOH$. *J. Chem. Soc., Dalton Trans.* **1997**, 1633−1637. (d) Marchetti, F.; Pampaloni, G.; Zacchini, S. The reactivity of $MoCl_5$ with molecules containing the alcohol functionality. *Polyhedron* **2015**, *85*, 369−375.

(12) Rillema, D. P.; Brubaker, C. H. Complexes of Molybdenum(V) and Tungsten(V). Far-Infrared Sprectra and Some Other Properties. *Inorg. Chem.* **1969**, *8*, 1645−1649.

(13) A similar mechanism might be operative in the deoxygenation of $Ph_3P{=}O$ or DMSO; see the following: Horner, S. M.; Tyree, S. Y. The Reaction of Some Oxygen Donors with Molybdenum Pentachloride: Coordination Compounds of Molybdenum(V) Oxytrichloride and Molybdenum(VI) Dioxydichloride. *Inorg. Chem.* **1962**, *1*, 122−127.

(14) Cotton, F. A; Wilkinson, G.; Murillo, C. A.; Bochmann, M. *Advanced Inorganic Chemistry*, 6th ed.; Wiley: New York, 1999.

(15) A few homoleptic Mo(VI) alkoxides are known; see the following: (a) Jacob, E. Metallhexamethoxide. *Angew. Chem.* **1982**, *94*, 146−147. (b) Seisenbaeva, G. A.; Kloo, L.; Werndrup, P.; Kessler, V. G. Electrochemical Synthesis, X-ray Single Crystal, IR Spectroscopic and Quantum Chemical Investigation of Molybdenum and Tungsten Hexamethoxides. *Inorg. Chem.* **2001**, *40*, 3815−3818. (c) Buth, S.; Wocadlo, S.; Neumüller, B.; Weller, F.; Dehnicke, K. Synthese und Kristallstrukturen von Tris(glycolateo)molybdän(VI) und Tris-(pinakolato)molybdän(VI). *Z. Naturforsch., B: J. Chem. Sci.* **1992**, *47b*, 706−712.

(16) See the following for leading references and literature cited therein: (a) Mitchell, P. C. H. Oxo-species of molybdenum-(V) and -(VI). *Q. Rev., Chem. Soc.* **1966**, *20*, 103−118. (b) Braithwaite, E. R.; Haber, J., Eds. *Molybdenum: An Outline of its Chemistry and Uses. Studies in Inorganic Chemistry*; Elsevier: Amsterdam, 1994; Vol. *19*. (c) Sousa, S. C. A.; Cabrita, I.; Fernandes, A. C. High-valent oxo-molybdenum and oxo-rhenium complexes as efficient catalysts for X-H (X = Si, B, P or H) bond activation and for organic reductions. *Chem. Soc. Rev.* **2012**, *41*, 5641−5653. (d) Arzoumanian, H. Molybdenum-Oxo and Peroxo Complexes in Oxygen Atom Transfer Processes with O_2 as the Primary Oxidant. *Curr. Inorg. Chem.* **2011**, *1*, 140−145. (e) Karunadasa, H. I.; Chang, C. J.; Long, J. R. A molecular molybdenum-oxo catalyst for generating hydrogen from water. *Nature* **2010**, *464*, 1329−1333.

(17) (a) Coughlan, M. P., Ed. *Molybdenum and Molybdenum-Containing Enzymes*; Pergamon Press: Oxford, 1980. (b) Hille, R.; Rétey, J.; Bartlewski-Hof, U.; Reichenbecher, W.; Schink, B.

Mechanistic aspects of molybdenum containing enzymes. *FEMS Microbiol. Rev.* **1998**, *22*, 489−501. (c) Groysman, S.; Holm, R. H. Biomimetic Chemistry of Iron, Nickel, Molybdenum and Tungsten in Sulfur-Ligated Protein Sites. *Biochemistry* **2009**, *48*, 2310−2320. (d) Hille, R.; Hall, J.; Basu, P. The Mononuclear Molybdenum Enzymes. *Chem. Rev.* **2014**, *114*, 3963−4038.

(18) Schubert, M.; Leppin, J.; Wehming, K.; Schollmeyer, D.; Heinze, K.; Waldvogel, S. R. Powerful Fluoroalkoxy Molybdenum(V) Reagent for Selective Oxidative Arene Coupling Reaction. *Angew. Chem., Int. Ed.* **2014**, *53*, 2494−2497.

(19) Complex **6** dissociates partly in CH_2Cl_2 and fully in trifluoroethanol (*cf.* ref 18); in the solid state, it is diamagnetic and shows a short Mo−Mo distance (2.832 Å), which suggests metal−metal bonding/antiferromagnetic spin coupling, although this aspect has not been addressed in the original publication. A single bond between the metal centers was proposed for the related complex **7** featuring a similar Mo−Mo distance (2.8077 Å) (*cf.* ref 20); therefore, **6** is also drawn in Scheme 1 with a Mo−Mo bond.

(20) Bardina, N. V.; Bazhenova, T. A.; Lyssenko, K. A.; Antipin, M. Y.; Shulga, Y. M.; Filina, T. A.; Shestakov, A. F. Unusual binuclear alkoxomolybdenum(V) complex free of oxo groups: synthesis, structure and IR spectra. *Mendeleev Commun.* **2006**, *16*, 307−308.

(21) The plethora of complexes formed on treatment of $MoCl_5$ with methanol/methoxide is representative; see the following: Bazhenova, T. A.; Lyssenko, K. A.; Kuznetsov, D. A.; Kovaleva, N. V.; Manakin, Y. V.; Savinykh, T. A.; Shestakov, A. F. Methanolyis of $MoCl_5$ in the Presence of Different Alkaline Agents; Molecular Structures of the Polynuclear Molybdenum(V) Methoxides and Electron Charge Densitry Distribution from X-ray Diffraction Study of the New K-Mo Cluster. *Polyhedron* **2014**, *76*, 108−116.

(22) In addition to various ethers, benzene, and MeCN, simple olefins (norbornene, allyltrimethylsilane, tetrachloroethane) were employed to prepare lower-valent molybdenum species; of course, silanes, Zn, Sn, Al, $SnCl_2$, organolithium, and organozinc reagents can also be used as reducing agents. For an overview, see ref 8 and the following reference, including the literature cited therein: Persson, C.; Andersson, C. Reduction of tungsten(VI) and molybdenum(V) by allyltrimethylsilane and cyclopentene. Simple high yield syntheses of $MoCl_4(OEt_2)_2$, $MoCl_4$(dme), $WCl_4(thf)_2$, WCl_4(dme) and $WOCl_3(thf)_2$. *Inorg. Chim. Acta* **1993**, *203*, 235−238.

(23) There is evidence for both mechanisms; see the following: (a) Chisholm, M. C.; Folting, K.; Huffman, J. C.; Kirkpatrick, C. C. Reactions of Metal-Metal Multiple Bonds. 10. Reactions of $Mo_2(OR)_6$ (M≡M) and $[Mo(OR)_4]_x$ Compounds with Molecular Oxygen. Preparation and Characterization of Oxo Alkoxides of Molybdenum: $MoO_2(OR)_2$, $MoO_2(OR)_2$(bpy), $MoO(OR)_4$, $Mo_3O(OR)_{10}$, $Mo_4O_8(OR)_4(py)_4$, and $Mo_6O_{10}(OR)_{12}$. *Inorg. Chem.* **1984**, *23*, 1021−1037. (b) Mayer, J. M. Not Solely a Spectator: Exploring the Chemistry of the C-O Bond in Alkoxide and Related Ligands. *Polyhedron* **1995**, *14*, 3273−3292.

(24) Peters, J. C.; Johnson, A. R.; Odom, A. L.; Wanandi, P. W.; Davis, W. M.; Cummins, C. C. Assembly of Molybdenum/Titanium μ-Oxo Complexes via Radical Alkoxide C-O Cleavage. *J. Am. Chem. Soc.* **1996**, *118*, 10175−10188.

(25) Cotton, F. A.; Murillo, C. A. *Multiple Bonds Between Metal Atoms*, 3rd ed.; Walton, R. A., Ed.; Springer: New York, 2005.

(26) Homoleptic, low-valent, and monomeric Mo complexes are known; for classical case studies, see the following: (a) Kuiper, D. S.; Wolczanski, P. T.; Lobkovsky, E. B.; Cundari, T. R. Low Coordinate, Monomeric Molybdenum and Tungsten (III) Complexes: Structure, Reactivity and Calculational Studies of $(silox)_3$Mo and $(silox)_3$ML (M = Mo, W; L = PMe_3, CO; silox = $^tBu_3SiO$). *J. Am. Chem. Soc.* **2008**, *130*, 12931−12943. (b) Schrock, R. R. Catalytic Reduction of Dinitrogen to Ammonia at a Single Molybdenum Center. *Acc. Chem. Res.* **2005**, *38*, 955−962. (c) Cummins, C. C. Reductive Cleavage and Related Reactions Leading to Molybdenum-Element Multiple Bonds: New Pathways Offered by Three-coordinate Molybdenum(III). *Chem. Commun.* **1998**, 1777−1786.

(27) For representative examples, see the following: (a) Chisholm, M. H.; Huffman, J. C.; Kramer, K. S.; Streib, W. E. $Mo_4(H)_3(O\text{-}t\text{-}Bu)_7(HNMe_2)$: A Novel Hydrido Cluster of Molybdenum. *J. Am. Chem. Soc.* **1993**, *115*, 9866−9867. (b) Chisholm, M. H.; Hoffman, D. M.; McCandless Northius, J.; Huffman, J. C. Further studies of the reactions involving ethyne and $M_2(OtBu)_6$, where M = Mo and W. Polyacetylene formation versus formation of ethyne adducts and C-C coupled products. *Polyhedron* **1997**, *16*, 839−847.

(28) Chisholm, M. H.; Reichert, W. W.; Thornton, P. Tetrakis-(alkoxy) and Tetrakis(trialkylsiloxy) Compounds of Molybdenum-(IV). *J. Am. Chem. Soc.* **1978**, *100*, 2744−2748.

(29) Stoffelbach, F.; Saurenz, D.; Poli, R. Improved Preparations of Molybdenum Coordination Compounds from Tetrachlorobis(diethyl ether)molybdenum(IV). *Eur. J. Inorg. Chem.* **2001**, *2001*, 2699−2703.

(30) (a) Fürstner, A. Alkyne Metathesis on the Rise. *Angew. Chem., Int. Ed.* **2013**, *52*, 2794−2819. (b) Fürstner, A.; Davies, P. W. Alkyne Metathesis. *Chem. Commun.* **2005**, 2307−2320.

(31) Fürstner, A. Teaching Metathesis "Simple" Stereochemistry. *Science* **2013**, *341*, 1229713.

(32) Ehrhorn, H.; Tamm, M. Well-Defined Alkyne Metathesis Catalysts: Developments and Recent Applications. *Chem. - Eur. J.* **2019**, *25*, 3190−3208.

(33) (a) McCullough, L. G.; Schrock, R. R. Metathesis of Acetylenes by Molybdenum(VI) Alkylidyne Complexes. *J. Am. Chem. Soc.* **1984**, *106*, 4067−4068. (b) McCullough, L. G.; Schrock, R. R.; Dewan, J. C.; Murdzek, J. C. Preparation of Trialkoxymolybdenum(VI) Alkylidyne Complexes, Their Reactions with Acetylenes, and the X-ray Structure of $Mo(C_3(CMe_3)_2][OCH(CF_3)_2]_2(C_5H_5N)_2$. *J. Am. Chem. Soc.* **1985**, *107*, 5987−5998.

(34) (a) Fürstner, A.; Mathes, C.; Lehmann, C. W. $Mo[N(t\text{-}Bu)(Ar)]_3$ Complexes as Catalyst Precursors: In Situ Activation and Application to Metathesis Reactions of Alkynes and Diynes. *J. Am. Chem. Soc.* **1999**, *121*, 9453−9454. (b) Fürstner, A.; Mathes, C.; Lehmann, C. W. Alkyne Metathesis: Development of a Novel Molybdenum-based Catalyst System and its Application to the Total Synthesis of Epothilone A and C. *Chem. - Eur. J.* **2001**, *7*, 5299−5317.

(35) Zhang, W.; Lu, Y.; Moore, J. S. Preparation of a Triamidomolybdenum(VI) Propylidyne Complex − A Highly Active Catalyst Precursor for Alkyne Metathesis. *Org. Synth.* **2007**, *84*, 163−176.

(36) (a) Heppekausen, J.; Stade, R.; Goddard, R.; Fürstner, A. Practical New Silyloxy-based Alkyne Metathesis Catalysts with Optimized Activity and Selectivity Profiles. *J. Am. Chem. Soc.* **2010**, *132*, 11045−11057. (b) Heppekausen, J.; Stade, R.; Kondoh, A.; Seidel, G.; Goddard, R.; Fürstner, A. Optimized Synthesis, Structural Investigation, Ligand Tuning and Synthetic Evaluation of Silyloxy-based Alkyne Metathesis Catalysts. *Chem. - Eur. J.* **2012**, *18*, 10281−10299. (c) Schaubach, S.; Gebauer, K.; Ungeheuer, F.; Hoffmeister, L.; Ilg, M. K.; Wirtz, C.; Fürstner, A. A Two-Component Alkyne Metathesis Catalyst System with an Improved Substrate Scope and Functional Group Tolerance: Development and Applications to Natural Product Synthesis. *Chem. - Eur. J.* **2016**, *22*, 8494−9507.

(37) (a) Hillenbrand, J.; Leutzsch, M.; Yiannakas, E.; Gordon, C. P.; Wille, C.; Nöthling, N.; Copéret, C.; Fürstner, A. Canopy Catalysts" for Alkyne Metathesis: Molybdenum Alkylidyne Complexes with a Tripodal Ligand Framework. *J. Am. Chem. Soc.* **2020**, *142*, 11279−11294. (b) Hillenbrand, J.; Leutzsch, M.; Fürstner, A. Molybdenum Alkylidyne Complexes with Tripodal Silanolate Ligands: the Next Generation of Alkyne Metathesis Catalysts. *Angew. Chem., Int. Ed.* **2019**, *58*, 15690−15696.

(38) Haberlag, B.; Wu, X.; Brandhorst, K.; Grunenberg, J.; Daniliuc, C. G.; Jones, P. G.; Tamm, M. Preparation of Imidazolin-2-iminato Molybdenum and Tungsten Benzylidyne Complexes: A New Pathway to Highly Active Alkyne Metathesis Catalysts. *Chem. - Eur. J.* **2010**, *16*, 8868−8877.

(39) Bindl, M.; Stade, R.; Heilmann, E. K.; Picot, A.; Goddard, R.; Fürstner, A. Molybdenum Nitride Complexes with Ph_3SiO Ligands are Exceedingly Practical and Tolerant Precatalysts for Alkyne

https://dx.doi.org/10.1021/jacs.0c07073
J. Am. Chem. Soc. 2020, 142, 16392−16402

Metathesis and Efficient Nitrogen Transfer Agents. *J. Am. Chem. Soc.* **2009**, *131*, 9468−9470.
(40) (a) Cummins, C. C. Reductive cleavage and related reactions leading to molybdenum-element multiple bonds: new pathways offered by three-coordinate molybdenum(III). *Chem. Commun.* **1998**, 1777−1786. (b) Laplaza, C. E.; Johnson, M. J. A.; Peters, J. C.; Odom, A. L.; Kim, E.; Cummins, C. C.; George, G. N.; Pickering, I. J. Dinitrogen Cleavage by Three-Coordinate Molybdenum(III) Complexes: Mechanistic and Structural Data. *J. Am. Chem. Soc.* **1996**, *118*, 8623−8638.
(41) The use of coarse tin facilitates product isolation; *cf.* the following: Poli, R.; Gordon, J. C. ^{1}H NMR Investigation of the Tetrahydrofuran Replacement by Phosphine Ligands on $MoCl_3(THF)_3$. A Trans Effect. *Inorg. Chem.* **1991**, *30*, 4550−4554.
(42) Chisholm, M.; Cotton, F. A.; Murillo, C. A.; Reichert, W. W. The Molybdenum-Molybdenum Triple Bond. 2. Hexakis(alkoxy)-dimolybdenum Compounds: Preparation, Properties, and Structural Characterization of $Mo_2(OCH_2CMe_3)_6$. *Inorg. Chem.* **1977**, *16*, 1801−1808.
(43) Broderick, E. M.; Browne, S. C.; Johnson, M. J. A.; et al. Dimolybdenum and Ditungsten Hexa(Alkoxides). *Inorg. Synth.* **2014**, *36*, 95−102.
(44) ^{95}Mo NMR was used as an additional probe to confirm the formation of **8** (see the SI); the shift of δ_{Mo} = 2640 ppm in [D_8] toluene corresponds very well with the shift of δ_{Mo} = 2645 ppm reported in the literature; see the following: Young, C. G.; Kober, E. M.; Enemark, J. H. ^{95}Mo and ^{183}W NMR Studies on Triply Bonded Dinuclear M(III) and Related M≡C (M = Mo or W) Complexes. *Polyhedron* **1987**, *6*, 255−259.
(45) A brown/black precipitate starts to form at 50°C in [D_8] toluene; the decomposition becomes very fast when the temperature is further increased (see the Supporting Information); isobutene was the only detectable byproduct.
(46) The diffraction data had to be recorded at 200 K because the single crystals cracked upon further cooling.
(47) Certain analogies with monomeric $MoCl_5$ are noteworthy. At high temperature, $MoCl_5$ populates a trigonal bipyramidal (D_{3h}) and a square pyramidal form (C_{4v}) (some Mo_2Cl_{10} might also be present). In an argon or nitrogen matrix, only the C_{4v} geometry was observed; see the following: (a) Brunvoll, J.; Ischenko, A. A.; Spiridonov, V. P.; Strand, T. G. Composition and Molecular Structure of Gaseous Molybdenum Pentachloride by Electron Diffraction. *Acta Chem. Scand.* **1984**, *38A*, 115−120. (b) Brisdon, A. K.; Graham, J. T.; Hope, E. G.; Jenkins, D. M.; Levason, W.; Ogden, J. S. Spectroscopic Studies on Matrix-isolated Molybdenum Pentachloride. *J. Chem. Soc., Dalton Trans.* **1990**, 1529−1532. For a discussion of the possible Jahn−Teller distortion of the structure, see the following: (c) Bader, R. F. W.; Westland, A. D. The Electronic Spectra of $MoCl_5$ and $NbCl_5$. *Can. J. Chem.* **1961**, *39*, 2306−2315.
(48) The reported ^{1}H NMR signal of putative [Mo(O*t*Bu)$_4$] in C_6D_6 at 1.55 ppm is conspicuously close to that of [(*t*BuO)$_3$Mo≡Mo(O*t*Bu)$_3$], which resonates at 1.57 ppm in this solvent; see ref 43.
(49) Attempted formation of $[Mo(OtBu)_5]^+$ by chemical or electrochemical oxidation of **1** was unsuccessful; cyclovoltametric studies showed very broad and irreversible oxidation waves at ≈0.5 and ≈1.1 V; see the Supporting Information.
(50) We appreciate that the Mo−Mo distance per se is no reliable indicator; therefore, we refrain from assigning a bond order. While structurally remotely related but diamagnetic Mo complexes have previously been proposed to contain Mo═Mo bonds, the paramagnetic character of **9** renders a formal double bond unlikely. (a) Chisholm, M. H.; Cotton, F. A.; Extine, M. W.; Reichert, W. W. Structure and Bonding in Octaisopropoxydimolybdenum(IV). *Inorg. Chem.* **1978**, *17*, 2944−2946. (b) Chisholm, M. H.; Huffman, J. C.; Marchant, N. S. Reactions of M-M Triple Bonds with C-N Triple Bonds: Adduct Formation (M = Mo) and Metathesis (M = W) as Seen in the Reactions between Dimethylcyanamide and Hexaalkoxides of Dimolybdenum and Ditungsten. *J. Am. Chem. Soc.* **1983**, *105*, 6162−6163.
(51) Soo, H. S.; Figueroa, J. S.; Cummins, C. C. A Homoleptic Molybdenum(IV) Enolate Complex: Synthesis, Molecular and Electronic Structure, and NCN Group Transfer to Form a Terminal Cyanoimide of Molybdenum(VI). *J. Am. Chem. Soc.* **2004**, *126*, 11370−11376.
(52) Interestingly, ether-free $MoCl_4$ can be formed by compropotionation from $MoCl_5$ and $MoCl_3$ in a sealed tube, but it disproportionates back to these substrates upon heating to 120 °C in vacuum; see the following: (a) Couch, D. E.; Brenner, A. Preparation of Trichloride and Tetrachloride of Molybdenum. *J. Res. Natl. Bur. Stand., Sect. A* **1959**, *63A*, 185−188. (b) The disproportionation of amorphous $MoCl_4$ at 140 °C into $MoCl_5$ and $MoCl_3$ is described in ref 29.
(53) Complex **10** is analogous to complex **2**, which contains two THF ligands; see ref 6.
(54) (a) Cotton, F. A.; Su, J. The Solid State Structure and Solution Isomerization of $Mo_2Cl_6(THF)_3$. *Inorg. Chim. Acta* **1996**, *251*, 101−104. (b) Poli, R.; Mui, H. D. True Nature of Trihalotris-(tetrahydrofuran)molybdenum(III), $MoX_3(THF)_3$ (X = Cl, Br, I). A Paramagnetic ^{1}H Nuclear Magnetic Resonance Study. *J. Am. Chem. Soc.* **1990**, *112*, 2446−2448.
(55) The arguably closest case is found in the behavior of various tungsten halide species of different oxidation states on treatment with $LiNMe_2$; the resulting samples comprised the W(VI) and W(III) complexes $W(NMe_2)_6$ and $W_2(NMe_2)_6$, respectively, in the same unit cell in varying proportions. In the current context it is interesting to note, however, that [$WCl_4(THF)_2$] gave *pure* $W(NMe_2)_6$, whereas solvent-free [WCl_4] furnished *pure* $W_2(NMe_2)_6$ for reasons that remained entirely unclear. See the following: Chisholm, M. H.; Cotton, F. A.; Extine, M.; Stults, B. R. The Tungsten-Tungsten Triple Bond. 1. Preparation, Properties, and Structural Characterization of Hexakis(dimethylamido)-ditungsten(III) and Some Homologues. *J. Am. Chem. Soc.* **1976**, *98*, 4477−4485.
(56) Westphal, A.; Broda, H.; Kurz, P.; Neese, F.; Tuczek, F. Magnetic Circular Dichroism Spectrum of the Molybdenum(V) Complex [Mo(O)Cl$_3$dppe]: C-Term Signs and Intensities for Multideterminant Excited Doublet States. *Inorg. Chem.* **2012**, *51*, 5748−5763.
(57) Neese, F. High-Level Spectroscopy, Quantum Chemistry, and Catalysis: Not just a Passing Fad. *Angew. Chem., Int. Ed.* **2017**, *56*, 11003−11010.
(58) Wagner, J. P.; Schreiner, P. R. London Dispersion in Molecular Chemistry - Reconsidering Steric Effects. *Angew. Chem., Int. Ed.* **2015**, *54*, 12274−12296.
(59) For another unusual homoleptic complex formed by a disproportionation reaction that might be driven by dispersive forces between the ligands, see the following: Casitas, A.; Rees, J. A.; Goddard, R.; Bill, E.; DeBeer, S.; Fürstner, A. Two Exceptional Homoleptic Iron(IV) Tetraalkyl Complexes. *Angew. Chem., Int. Ed.* **2017**, *56*, 10108−10113.

https://dx.doi.org/10.1021/jacs.0c07073
J. Am. Chem. Soc. 2020, 142, 16392−16402